Islamic University of Technology (IUT)

Modeling and Small Signal Analysis of a Grid Connected Doubly Fed Induction Generator

by

Rifat Md. Bakhtear Biswas (102461)

Tonmoy Islam (102469)

Hasan M. Fazle Rabbi (102439)

Supervised by

Ashik Ahmed
Asst. Professor
Dept. of Electrical and Electronic Engineering (EEE)

A Dissertation

Submitted in Partial Fulfillment of the Requirement for the
Bachelor of Science in Electrical and Electronic Engineering
Academic Year: 2013-2014

Department of Electrical and Electronic Engineering (EEE)
Islamic University of Technology (IUT)
The Organization of Islamic Cooperation (OIC)
Gazipur-1704, Dhaka, Bangladesh

Modeling and Small Signal Analysis of a Grid Connected Doubly Fed Induction Generator

A thesis presented to
The Academic Faculty
by

Rifat Md. Bakhtear Biswas (102461)
Tonmoy Islam (102469)
Hasan M. Fazle Rabbi (102439)

Approved by
Ashik Ahmed

……
Ashik Ahmed
Project Supervisor
Dept. Of Electrical and Electronic Engineering

……
Prof. Dr. Md. ShahidUllah
Head of the Department
Dept. Of Electrical and Electronic Engineering

Members:

……..
Rifat Md. Bakhtear Biswas

……
Tonmoy Islam

…….
Hasan M. Fazle Rabbi

Islamic University of Technology (IUT)
The Organization of Islamic Cooperation (OIC)
Gazipur-1704, Dhaka, Bangladesh
November - 2014

Declaration

This is to certify that the project entitled "**Modeling and Small Signal Analysis of a Grid Connected Doubly Fed Induction Generator'** is supervised by Ashik Ahmed. This project work has not been Submitted anywhere for a degree.

……
Ashik Ahmed
Project Supervisor
Dept. Of Electrical and Electronic Engineering

…….. ……
Rifat Md. Bakhtear Biswas Tonmoy Islam

…….
Hasan M. Fazle Rabbi

Acknowledgements

First of all, we would like to express our deep and sincere gratitude to our respected supervisor **Ashik Ahmed,** Assistant Professor in Electrical and Electronic Engineering department of Islamic University of Technology (IUT), Dhaka, Bangladesh, for his kind guidance and supervision on the thesis work. His regular and well supervision, kind helps, patience made this thesis gain its goal.

Second, we would like to express our deepest cordial thanks to all of our teachers for their supports and helpful attitude without which this thesis work might not bear fruit.

Finally we would like to thank to our parents who gave us hopes and inspirations.

Abstract

Wind power, as an alternative to fossil fuels, is plentiful, renewable, widely distributed, clean, produces no greenhouse gas emissions during operation and uses little land. Unlike other sources of electricity that require fuel in processing plants, wind energy generates electricity through wind, which is free. So wind turbines might be used jointly with conventional generation system to contribute to the grid. But this practice can affect the stability of the conditions of the power system. Hence, we need to contemplate the power system stability conditions when DFIG power plant appended to it.

This thesis describes the modeling and small signal analysis of a grid connected doubly-fed induction generator (DFIG). The model was developed from the basic flux linkage, voltage and torque equations. The change in properties for different system parameters, operating points, and grid strengths are computed and observed. The results offer a better understanding of the DFIG intrinsic dynamics, which can also be useful for control design and model justification.

Keywords

Doubly-fed induction generator, DFIG, small-signal model, eigenvalue analysis, small-signal stability, non-linear dynamic model

Contents

List of Tables

Chapter 1

Introduction

1.1 Introduction

Wind energy is gaining increasing importance throughout the world. This fast development of wind energy technology and of the market has large implications for a number of people and institutions: for instance, for scientists who research and teach future wind power and electrical engineers at universities; for professionals at electric utilities who really need to understand the complexity of the positive and negative effects that wind energy can have on the power system; for wind turbine manufacturers; and for developers of wind energy projects, who also need that understanding in order to be able to develop feasible, modern and cost-effective wind energy projects. Currently, five countries – Germany, USA, Denmark, India and Spain – concentrate more than 83% of worldwide wind energy capacity in their countries [10].

With the worldwide trend and wish to integrate more wind energy into the power system, there has been an urgent need of suitable dynamical models of wind generators. As control design is a major concern, a small-signal analysis can give valuable information on the DFIG properties, limitations and control options. This thesis presents the small-signal analysis of a grid connected doubly-fed induction generator (DFIG). To this end, the system non-linear dynamical model is derived. Then, its linearization and eigenvalue analysis are presented.

As an initiative, this thesis first considers a single machine infinite-bus system and investigates the stability conditions with and without disturbance. Afterwards, a DFIG is considered to be connected to the infinite-bus system along with the single machine and the power system stability is examined once more.

1.2 Power system stability

Power system stability may be defined as that property of the system which enables the synchronous machines of the system to respond to a disturbance from a normal operating condition so as to return to a condition where their operation is again normal.

The power system stability is divided is divided in two classes:

1. Steady state stability

   The steady state stability of a power system is defined as the ability of the system to bring itself back to its stable configuration following a small disturbance in the network.

   In case the power flow through the circuit exceeds the maximum power permissible, then there are chances that a particular machine or a group of machines will cease to operate in synchronism, and result in yet more disturbances. In such a situation, the steady state limit of the system is said to have reached. Or in other words the steady state stability limit of a system refers to the maximum amount of power that is permissible through the system without loss of its steady state stability.

2. Transient stability

   Transient stability of a power system refers to the ability of the system to reach a stable condition following a large disturbance in the network condition. In all cases related to large changes in the system like sudden application or removal of load, switching operations, line faults or loss due to excitation the transient stability of the system comes into play. It in fact deals in the ability of the system to retain synchronism following a disturbance sustaining for a reasonably long period of time.

   And the maximum power that is permissible to flow through the network without loss of stability following a sustained period of disturbance is referred to as the transient stability of the system. Going beyond that maximum permissible value for power flow, the system would temporarily be rendered as unstable.

1.3 Wind Turbine

A wind turbine is a device that converts kinetic energy from the wind into electrical power. A wind turbine is similar to a fan but works in reverse direction. Typically wind turbines are much larger in size as compared to a fan [11].

The result of over a millennium of windmill development and modern engineering, today's wind turbines are manufactured in a wide range of vertical and horizontal axis types. The smallest turbines are used for applications such as battery charging for auxiliary power for boats or caravans or to power traffic warning signs. Slightly larger turbines can be used for making small contributions to a domestic power supply. Arrays of large turbines, known as wind farms, are becoming an increasingly important source of renewable energy and are used by many countries as part of a strategy to reduce their reliance on fossil fuels.

1.3.1 Types of wind turbine

Wind turbines can rotate about either a horizontal or a vertical axis, the former being both older and more common [11].

1. **Horizontal-axis wind turbines**

   Horizontal-axis wind turbines (HAWT) have the main rotor shaft and electrical generator at the top of a tower, and must be pointed into the wind. Most have a gearbox, which turns the slow rotation of the blades into a quicker rotation that is more suitable to drive an electrical generator [11].

   Since a tower produces turbulence behind it, the turbine is usually positioned upwind of its supporting tower. Turbine blades are made stiff to prevent the blades from being pushed into the tower by high winds. Additionally, the blades are placed a considerable distance in front of the tower and are sometimes tilted forward into the wind a small amount.

2. **Vertical-axis wind turbine**

   Vertical-axis wind turbines (or VAWTs) have the main rotor shaft arranged vertically. One advantage of this arrangement is that the turbine does not need to be pointed into the wind to be effective, which is an advantage on a site where the wind direction is highly variable. It is also an advantage when the turbine is integrated into a building because it is inherently less steerable. Also, the generator and gearbox can be placed near the ground, using a direct drive from the rotor assembly to the ground-based gearbox, improving accessibility for maintenance.

1.3.2 Working principle of Wind turbine

Wind turbines use wind energy to produce electricity. The wind turbines are machines that have a rotor with three propeller blades. These blades are specifically arranged in a horizontal manner to propel wind for generating electricity. Wind turbines are placed in areas that have high speeds of wind, to spin the blades much quicker for the rotor to transmit the electricity produced to a generator.

Thereafter the electricity produced is supplied to different stations through the grid. One wind turbine can generate enough electricity to be used by a single household. A wind energy plant normally consists of many wind turbines that are 30 to 50m long each. According to the rule, the higher you go, the cooler it becomes and more air is circulated. This rule is applied by constructing turbines at high altitudes, to use the increased air circulation at high altitudes to propel the turbines much faster.

1.3.3 Components of wind turbine

The main components of a wind turbine for electricity generation are: rotor, transmission system and generator, yaw and control system. Apart from the rotor, most of the components are kept inside the 'nacelle' [11].

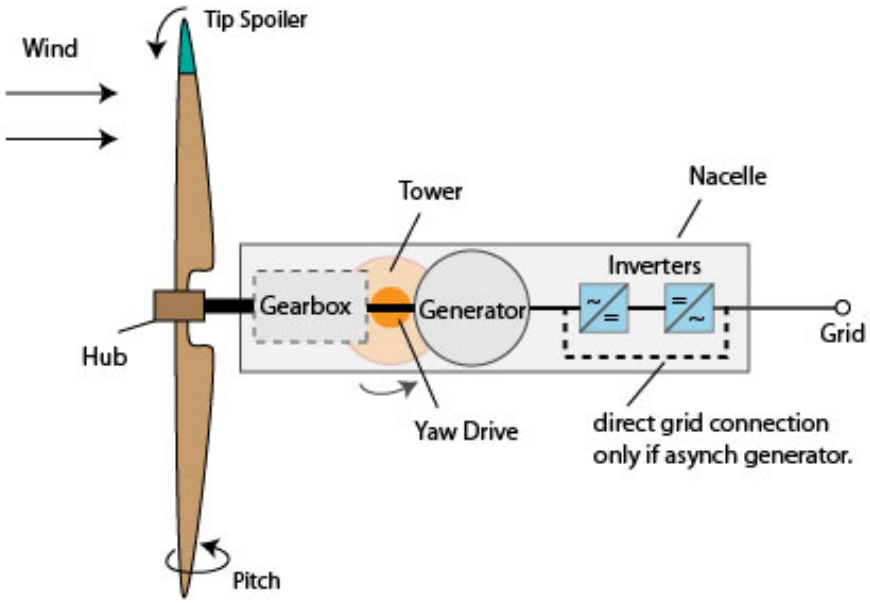

Fig.1.1 Components of wind turbine

1.4 Types of Wind Generator

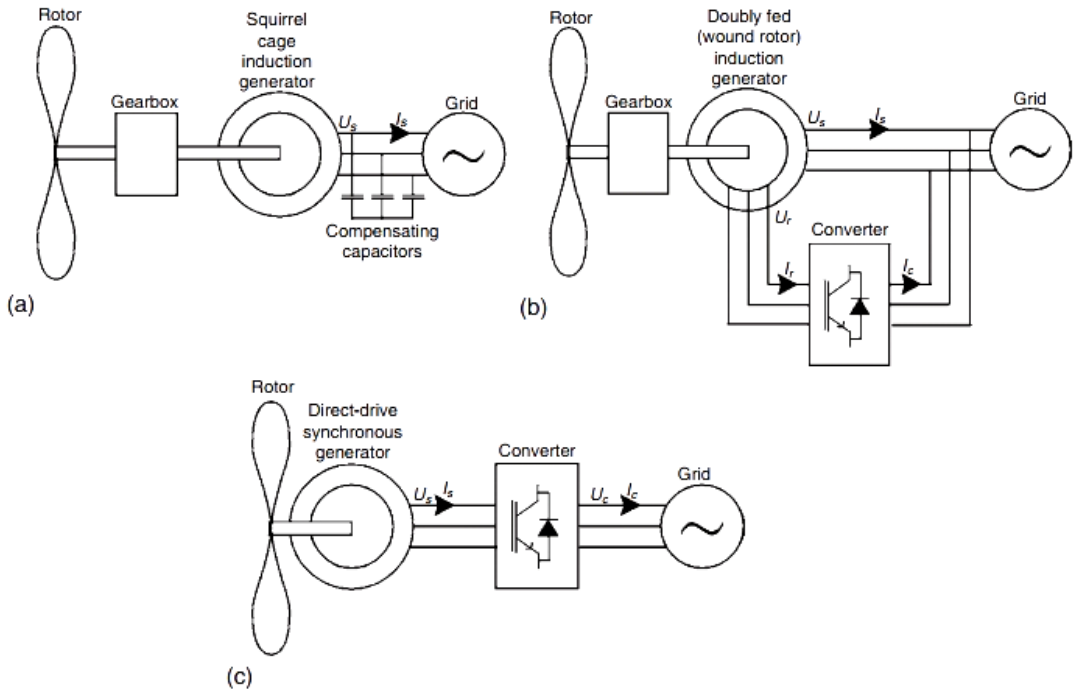

Fig.1.2 widely used wind turbine types: (a) constant-speed wind turbine (Type A); (b) variable-speed wind turbine with doubly fed induction generator (Type B); and (c) direct-drive variable-speed wind turbine with multi pole synchronous generator (Type C) [10]

1.5 Doubly-fed induction generator

The concept of variable speed with partial scale frequency converter is known as doubly fed induction generator (DFIG). Similar to the squirrel cage induction generator, it needs a gearbox. The stator winding of the generator is coupled to the grid, and the rotor winding to a power electronic converter, nowadays usually a back-to-back voltage source converter with current control loops. In this way, the electrical and mechanical rotor frequencies are decoupled, because the power electronic converter compensates the difference between mechanical and electrical frequency by injecting a rotor current with variable frequency. Variable-speed operation thus becomes possible. This means that the mechanical rotor speed can be controlled according to a certain goal function, such as energy yield maximization or noise minimization.

The rotor speed is controlled by changing the generator power in such a way that it equals the value derived from the goal function. In this type of conversion system, the control of aerodynamic power is usually performed by pitch control.

1.6 Method of simulation

In this thesis the non-linear model of single machine infinite-bus system and non-linear model of DFIG connected to infinite bus together with conventional generation are developed through equation. These models are then simulated using the software MATLAB.

After that, the stability conditions of the models are observed. The results offer a better understanding of the DFIG intrinsic dynamics.

1.7 Structure of the thesis

This thesis is divided into 4 chapters. The main objective and goal is highlighted in the abstract part of the thesis. The thesis starts with the analysis of the non-linear model of single machine infinite-bus system and ends with small signal analysis of DFIG.

In chapter 1, a brief discussion of the thesis work is given in the introduction. Then in chapter 2, the non-linear model of the single machine infinite bus system is analyzed. Afterwards, the noon-linear model of DFIG operating side by side to a conventional generator in a power system is investigated. The results and the graphs of these simulations are emerged in chapter 4.

Chapter 2

Modeling of Synchronous Generator

2.1 Modeling of a Synchronous Generator Connected To Infinite Bus:

A single machine connected to an infinite bus (SMIB) is although not so realistic but for simplicity that can be considered. The system considered is in fig 2.1. This shows the external network with two ports. One port is connected to generator terminals while the second port is connected to a voltage source $E_b\angle 0$. Both the magnitude E_b and the phase angle of the voltage source are assumed to be constant. Also there is no loss of generality in assuming the phase angle of bus voltage as zero.

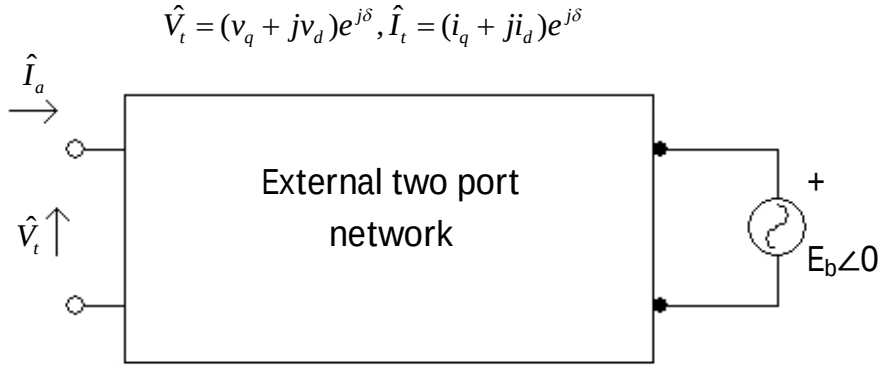

Fig.2.1 External two port network

The machine equations are:

$$\frac{d\delta}{dt} = \omega_B(S_m - S_{m0}) \quad (2.1)$$

$$\frac{dS_m}{dt} = \frac{1}{2H}[-D(S_m - S_{m0}) + T_m - T_e] \quad (2.2)$$

$$\frac{dE'_q}{dt} = \frac{1}{T'_{do}}[-E'_q + (x_d - x'_d)i_d + E_{fd}] \quad (2.3)$$

$$\frac{dE'_d}{dt} = \frac{1}{T'_{qo}}[-E'_d - (x_q - x'_q)i_q] \quad (2.4)$$

2.2 Initial conditions:

Initial conditions are given below,

$\hat{I}_{ao} = I_{ao}\angle\phi_0 = \frac{P_t - jQ_t}{V_{to}\angle -\theta_0}$ (2.5)

$E_{qo}\angle\delta_0 = V_{to}\angle\theta_0 + (R_a + jx_q)I_{ao}\angle\phi_0$ (2.6)

$i_{do} = I_{ao}\sin(\delta_0 - \theta_0)$ (2.7)

$i_{qo} = I_{ao}\cos(\delta_0 - \theta_0)$ (2.8)

$v_{do} = -v_{to}\sin(\delta_0 - \theta_0)$ (2.9)

$E_{fdo} = E_{qo} + (x_d - x_q)i_{do}$ (2.10)

$E'_{qo} = E_{qo} - (x_d - x'_d)i_{do}$ (2.11)

$E'_{do} = (x_q - x'_q)i_{qo}$ (2.12)

$T_{eo} = E'_{qo}i_{qo} + E'_{do}i_{do} + (x'_d - x'_q)i_{do}i_{qo} = T_{mo}$ (2.13)

2.3 Simulation for a system diagram

We added disturbance to simulate the real time disturbances occur in the practical network. Assume E_b = 1.0. We got the following curves for different cases. Different initial values for different cases are given below as a table,

Variable	Case(1)	Case(2)	Case(3)	Case(4)
δ	44.1	69.73	30.27	71.28
E'_q	1.111	0.6814	0.9312	0.3893
E'_d	-0.4568	-0.6126	-0.3273	-0.6245
i_d	-0.9332	-0.7813	-0.1536	-0.1535
i_q	0.3597	0.4835	0.2577	0.4838
E_{fd}	2.6787	2.0094	1.1923	0.6503
V_t	1.0928	0.9804	1.0022	0.9232

Table 2.1 Initial values for variation of P_t and Q_t

Case 1: Pt = 0.9, Qt = 0.6

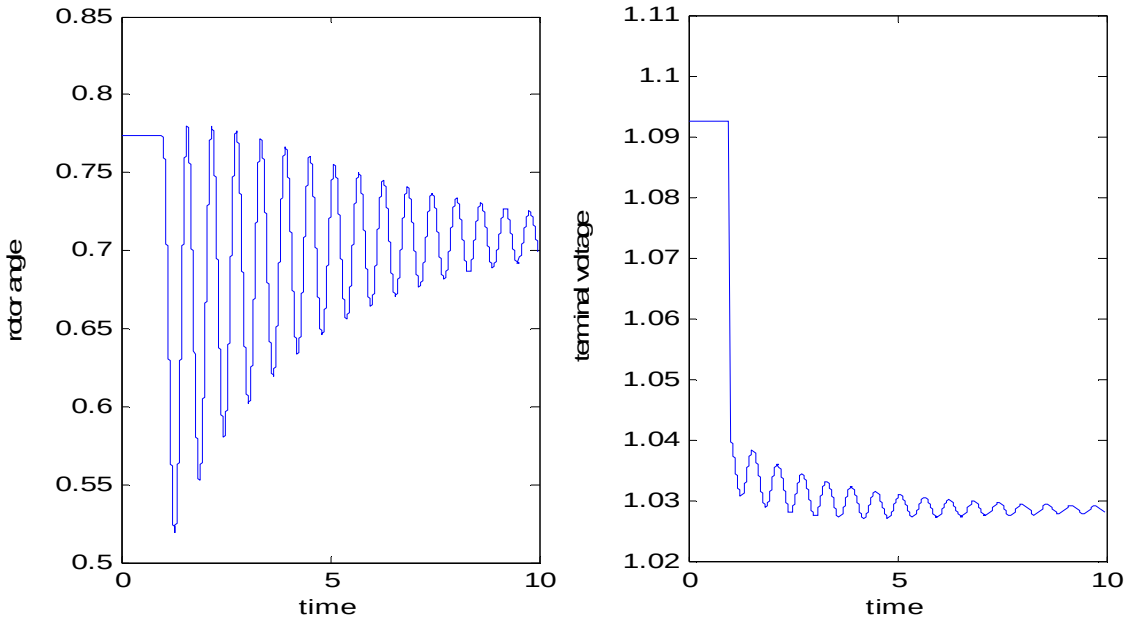

Fig.2.2 Swing curve and terminal voltage curve (case 1)

Case 2: Pt = 0.9, Qt = -0.02

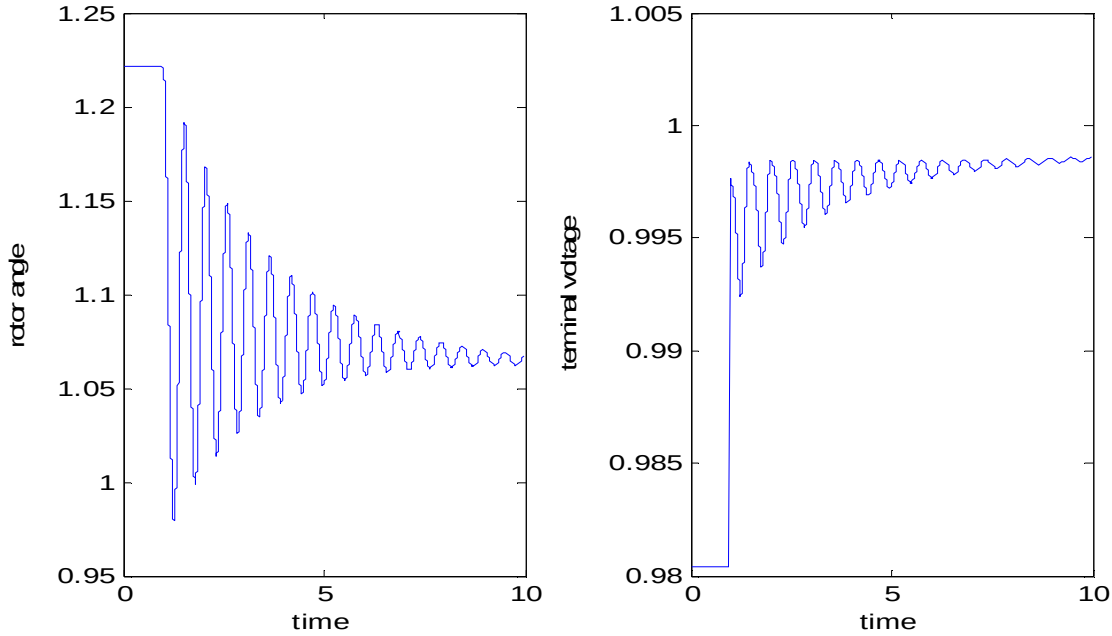

Fig.2.3 Swing curve and terminal voltage curve (case 2)

Case 3: Pt = 0.3, Qt = 0.02

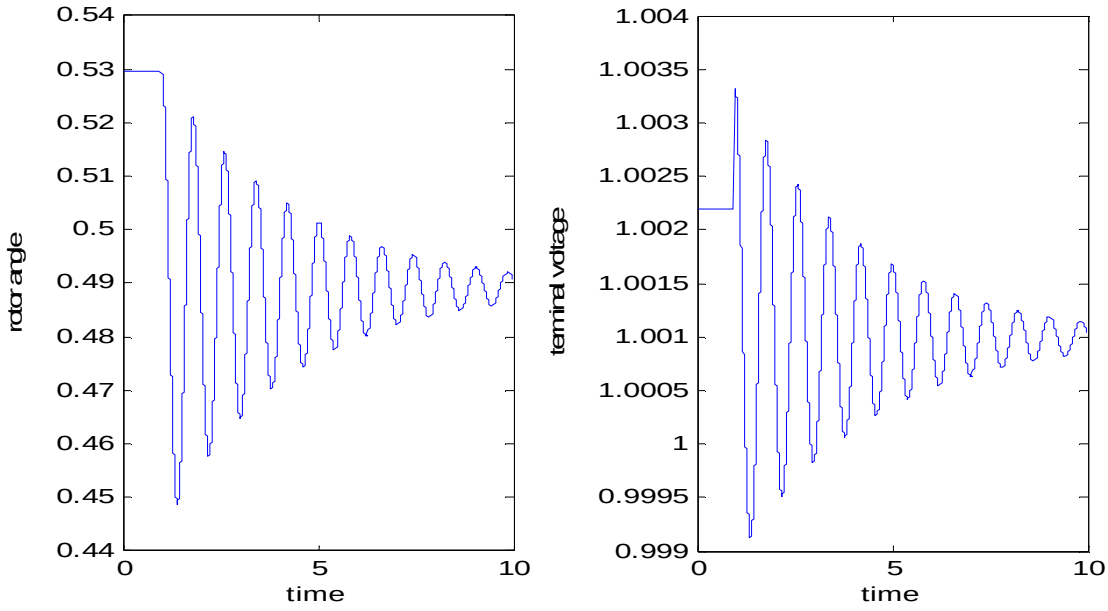

Fig.2.4 Swing curve and terminal voltage curve (case 3)

Case 4: Pt = 0.3, Qt = -0.36

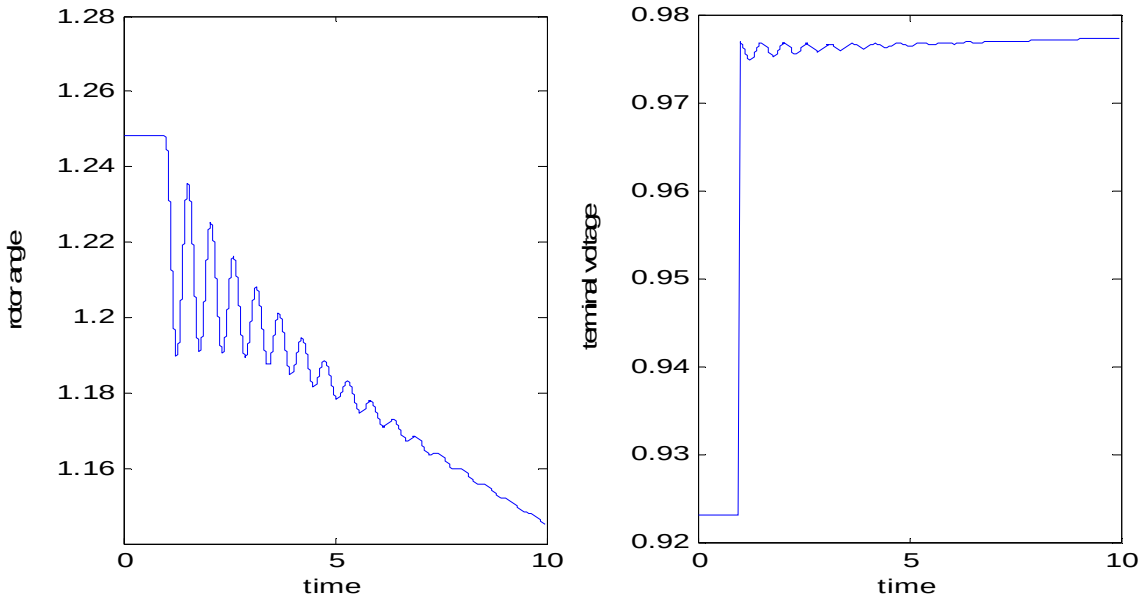

Fig.2.5 Swing curve and terminal voltage curve (case 4)

2.4 Analysis of single machine system

With classical model of the synchronous machine, the steady state instability at the limiting power is characterized by a slow monotonic increase (or decrease) in the rotor angle, resulting in loss of synchronism. With the advent of automatic voltage regulator (AVR) it was felt that steady state stability limit can be enhanced as the AVR acts to overcome the armature reaction. A simplified representation of the effect of AVR is the reduction of the generator reactance from x_d to a much smaller value. It is to be noted that without AVR, modern turbo-generators cannot operate at full rated power. Also, the transient stability is improved by fast acting exciters with high gain.

2.4.1 Small signal stability with block diagram representation

Consider a single machine system shown in Fig.2.6. For simplicity we will assume a synchronous machine represented by model 1.0 neglecting damper windings both in d and q axis. Also the armature resistance if the machine is neglected and the excitation system represented by a single time-constant system shown in Fig.2.7.

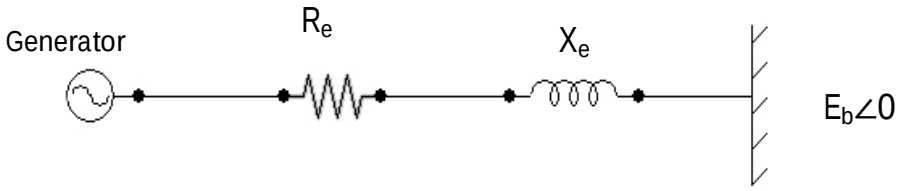

Fig.2.6 A single machine system

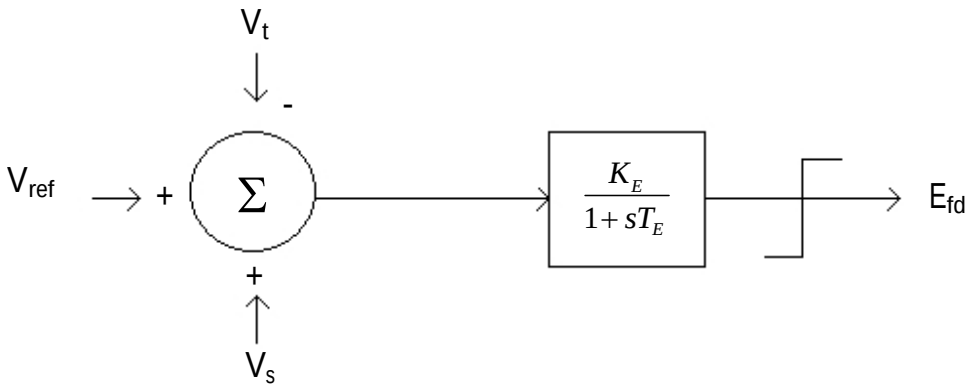

Fig.2.7 Excitation system

The algebraic equations of the stator are

$$E'_q + x'_d i_d = v_q \quad (2.14)$$

$$-x_q i_q = v_d \quad (2.15)$$

The complex terminal voltage can be expressed as

$$(v_q + jv_d) = (i_q + jid)(R_e + jx_e) + E_b e^{-j\delta} \quad (2.16)$$

Separating real and imaginary parts eq.(2.16) can be expressed as

$$v_q = R_e i_q - x_e i_d + E_b \cos\delta \quad (2.17)$$

$$v_d = R_e i_d + x_e i_q - E_b \sin\delta \quad (2.18)$$

Substituting eqs.(2.17) and (2.18) in eq.(2.14) and (2.15), we get,

$$\begin{pmatrix} (x'_d + x_e) & -R_e \\ R_e & -(x_q + x_e) \end{pmatrix} \begin{pmatrix} i_d \\ i_q \end{pmatrix} = \begin{pmatrix} E_b cos\delta - E'_q \\ -E_b sin\delta \end{pmatrix} \quad (2.19)$$

After linearizing we get,

$$\Delta i_d = C_1 \Delta\delta + C_2 \Delta E'_q \quad (2.20)$$

$$\Delta i_q = C_3 \Delta\delta + C_4 \Delta E'_q \quad (2.21)$$

Where

$C_1 = \frac{1}{A}[R_e E_b cos\delta_0 - (x_q + x_e) E_b sin\delta_0]$

$C_2 = -\frac{1}{A}(x_q + x_e)$

$C_3 = \frac{1}{A}[(x'_d + x_e) E_b cos\delta_0 + R_e E_b sin\delta_0]$

$C_4 = \frac{R_e}{A}$

Linearizing Eq.(2.14) and (2.15) and substituting from Eq. (2.20) and (2.21), we get,

$\Delta v_d = x'_d C_1 \Delta\delta + (1 + x'_d C_2)\Delta E'_q$ (2.22)

$\Delta v_q = -x_q C_3 \Delta\delta - x_q C_4 \Delta E'_q$ (2.23)

2.4.2 Rotor mechanical equation and torque angle loop

The rotor angle mechanical equations are

$$\frac{d\delta}{dt} = \omega_B (s_m - s_{m0}) \quad (2.24)$$

$$2H \frac{dS_m}{dt} = -DS_m + T_m - T_e \quad (2.25)$$

$$T_e = E'_q i_q - (x_q - x'_d) i_d i_q \quad (2.26)$$

After linearizing eq.(2.26) we get,

$\Delta T_e = K_1 \Delta\delta + K_2 \Delta E'_q$ (2.27)

Where

$K_1 = E_{q0} C_3 - (x_q - x'_d) i_{qo} C_1$ (2.28)

$K_2 = E_{q0} C_4 + i_{qo} - (x_q - x'_d) i_{qo} C_2$ (2.29)

$E_{qo} = E'_{q0} - (x_q - x'_d) i_{do}$ (2.30)

2.4.3 Representation of flux decay

The equation of field winding can be expressed as

$$T'_{do}\frac{dE'_q}{dt} = E_{fd} - E'_q + (x_d - x'_d)i_d \quad (2.31)$$

Linearizing the equation we get,

$$T'_{do}\frac{d\Delta E'_q}{dt} = \Delta E_{fd} - \Delta E'_q + (x_d - x'_d)(C_1\Delta\delta + C_2\Delta E'_q) \quad (2.32)$$

Taking laplace transform we get,

$$(1 + sT'_{do}K_3)\Delta E'_q = K_3\Delta E_{fd} - K_3K_4\Delta\delta \quad (2.33)$$

Where

$$K_3 = \frac{1}{[1-(x_d-x'_d)C_2]} \quad (2.34)$$

$$K_4 = -(x_d - x'_d)C_1 \quad (2.35)$$

2.4.4 Representation of Excitation system

The presentation of terminal voltage V_t can be expressed as,

$$\Delta V_t = \frac{v_{do}}{V_{to}}\Delta v_d + \frac{v_{qo}}{V_{to}}\Delta v_q \quad (2.36)$$

In general form

$$\Delta V_t = K_5\Delta\delta + K_6\Delta E'_q \quad (2.37)$$

Where

$$K_5 = \frac{v_{do}}{V_{to}}x_qC_3 + \frac{v_{qo}}{V_{to}}x'_dC_1 \quad (2.38)$$

$$K_6 = -\frac{v_{do}}{V_{to}}x_qC_4 + \left(\frac{v_{qo}}{V_{to}}\right)(1 - x'_dC_2) \quad (2.39)$$

2.4.5 Computation of Heffron-Philips Constants for Lossless Network

For R_e=0, the expressions for the constants K_1 to K_6 are simplified. As the armature resistance is already neglected, this refers to a lossless network on the stator side. The expressions are given below,

$$K_1 = \frac{E_b E_{qo} cos\delta_0}{(x_e+x_q)} + \frac{(x_q-x'_d)}{(x_e+x'_d)} E_b i_{q0} sin\delta_0 \quad (2.40)$$

$$K_2 = \frac{(x_e-x_q)}{(x_e+x'_d)} i_{qo} = \frac{E_b sin\delta_o}{(x_e+x'_d)} \quad (2.41)$$

$$K_3 = \frac{(x_e-x'_d)}{(x_e+x_d)} \quad (2.42)$$

$$K_4 = \frac{(x_d-x'_d)}{(x_e+x'_d)} E_b sin\delta_0 \quad (2.43)$$

$$K_5 = \frac{-x_q v_{do} E_b cos\delta_0}{(x_e+x_q)V_{to}} - \frac{x'_d v_{q0} E_b sin\delta_0}{(x_e+x'_d)V_{to}} \quad (2.44)$$

$$K_6 = \frac{x_e}{(x_e+x'_d)} \cdot \left(\frac{v_{q0}}{V_{to}}\right) \quad (2.45)$$

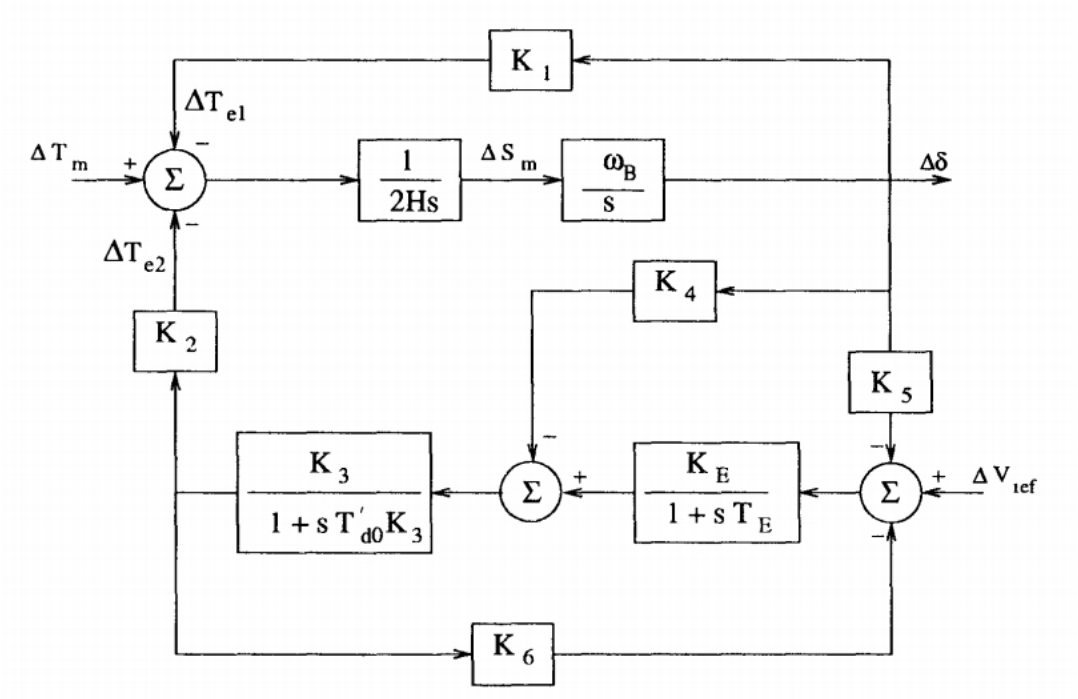

Fig.2.8 Overall block diagram

2.4.6 Simplified Model with State Equation

It is possible to express the system equations in the state space form. From the block diagram, fig.2.8 the following system equations can be derived

$$\dot{x} = [A]x + [B](\Delta V_{ref} + \Delta V_s) \tag{2.46}$$

Where

$$x = [\Delta\delta \quad \Delta S_m \quad \Delta E'_q \quad \Delta E_{fd}]$$

$$[A] = \begin{pmatrix} 0 & \omega_B & 0 & 0 \\ -\frac{K_1}{2H} & -\frac{D}{2H} & -\frac{K_2}{2H} & 0 \\ -\frac{K_4}{T'_{do}} & 0 & -\frac{1}{T'_{do}K_3} & \frac{1}{T'_{do}} \\ \frac{K_E K_5}{T_E} & 0 & -\frac{K_E K_6}{T_E} & -\frac{1}{T_E} \end{pmatrix}$$

$$[B] = \begin{bmatrix} 0 & 0 & 0 & \frac{K_E}{T_E} \end{bmatrix}$$

The dumping term D, is included in the swing equation. The eigenvalue of the matrix should lie in LHP in the 'S' plane for the system to be stable. The effect of various parameters (K_E and T_E) can be exclaimed from eigenvalue analysis. It is to be noted that the elements of matrix [A] are dependent on the operating condition.

2.4.7 Characteristics of Heffron-Phillip constants

The variations of K_1, ($K_1 - K_2K_3K_4$) and K_5 with variations in x_e for case (i)P_g = 0.5 and for case (ii) P_g = 1.0 are shown in fig.2.9. It is interesting to observe that,

i. $K_1>0$ for both cases. As expected, K_1 reduces with increase in x_e. The reduction is faster for case (b) Pg = 1.0.
ii. (K_1-$K_2K_3K_4$) is positive for case (a) while for case (b) it becomes negative foe x_e exceeding 0.7.
iii. $K_5>0$ for case (a) when $x_e<0.8$. However, $K_5<0$ for case (b) even for x_e = 0.1. K_5 reduces with increase in x_e.

If AVR is not considered then the conditions for stability are

$$K_1 > 0,\ K_1 - K_2K_3K_4 > 0$$

And if AVR is to be considered then the condition for stability is primarily,

$$K_E < \frac{K_4}{-K_5}$$

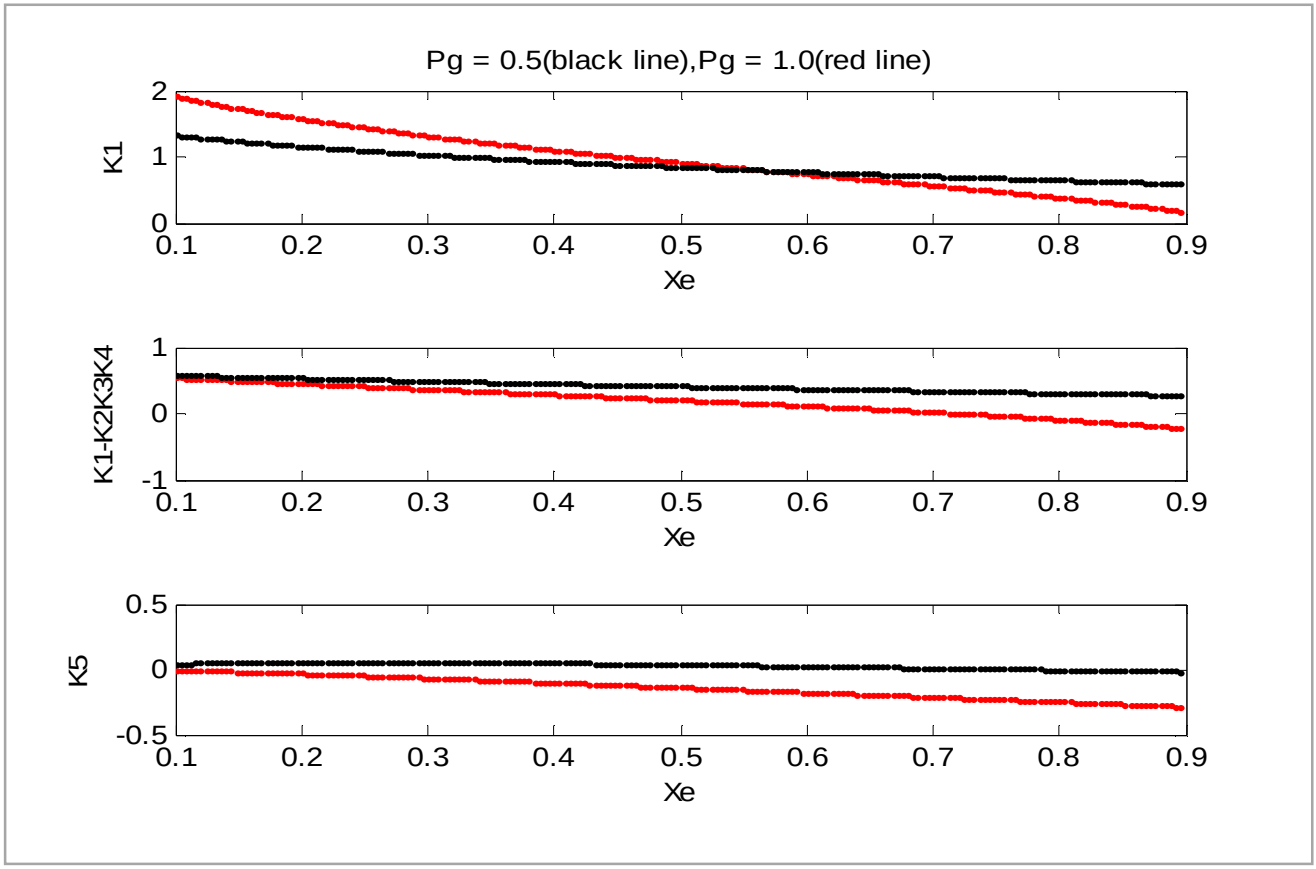

Fig.2.9 Variations of parameters with x_e

Again, the variations of K_1, (K_1-$K_2K_3K_4$) and K_5 with x_e = 0.4 and P_g varied from 0.5 to 1.5 is shown in fig.2.10. It is interesting to observe that,

i. K_1>0 and remains practically constant.
ii. (K_1-$K_2K_3K_4$) reduces with increase in P_g. It reaches the value of zero as P_g approaches 1.5p.u.
iii. K_5 reduces as P_g increases. K_5 crosses zero as P_g approaches the value of 0.7p.u. and remains negative as P_g is further increased.

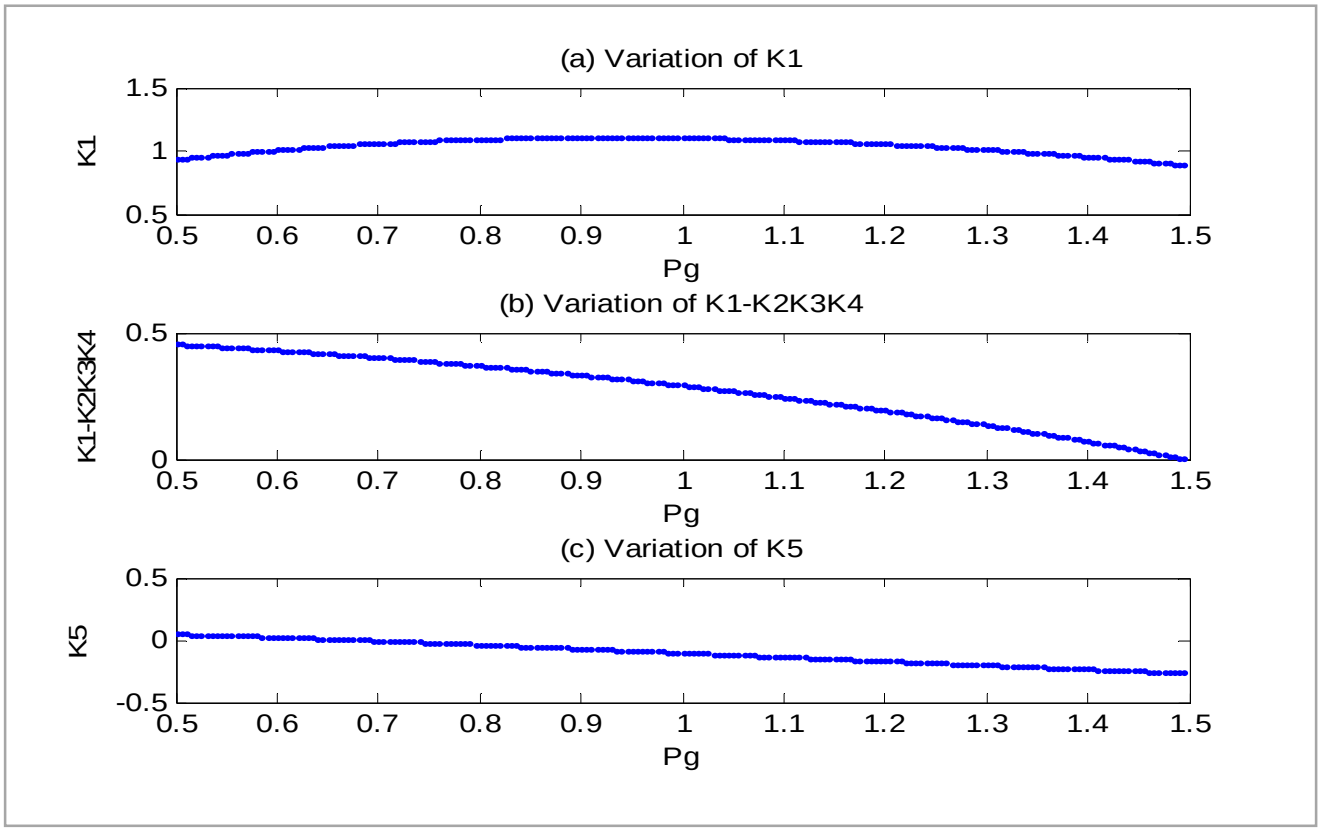

Fig.2.10. variations of parameters with P_g

2.5 Eigenvalue analysis

Suppose, A synchronous generator is connected to an infinite bus through an external reactance x_e=0.4p.u. and

(a) P_g = 0.5, V_t=1.0, E_b=1.0
(b) P_g = 1.0, V_t=1.0, E_b=1.0

We need to compute the eigenvalues for the two operating conditions and (i) without AVR and (ii) with AVR of T_E = 0.05 and K_E = 200.

The system matrix [A] is defined in eqn. 2.46. The substitutions of the parameter values and calculation of eigenvalues using MATLAb program gives the following results.

P_g	Without AVR	With AVR
0.5	-0.1185±j5.9302	-0.1512±j5.5407
	-0.2259	-10.0803±j14.3810

P_g	Without AVR	With AVR
1.0	-0.1702±j6.4518	0.5091±j7.1562
	-0.1225	-10.7405±j12.1037

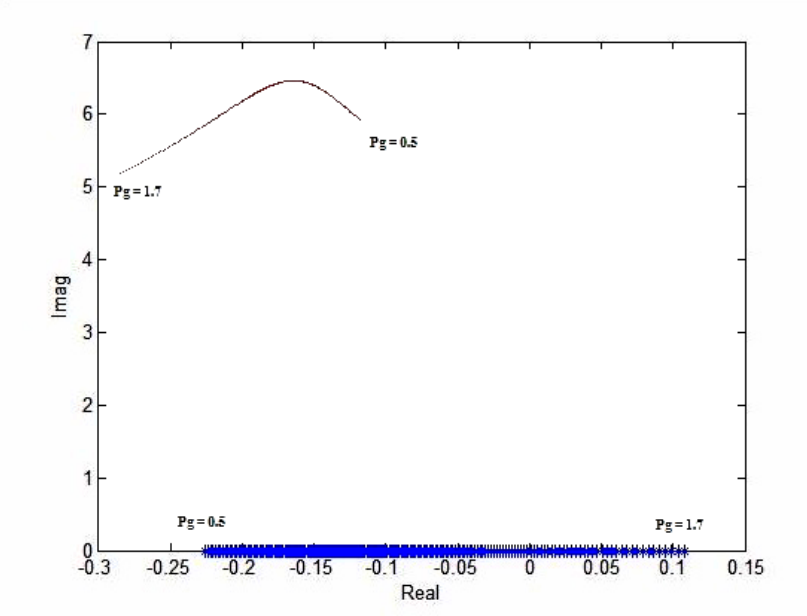

Fig.2.11 Eigenvalue loci for variation in P_g (0.5 – 1.7)

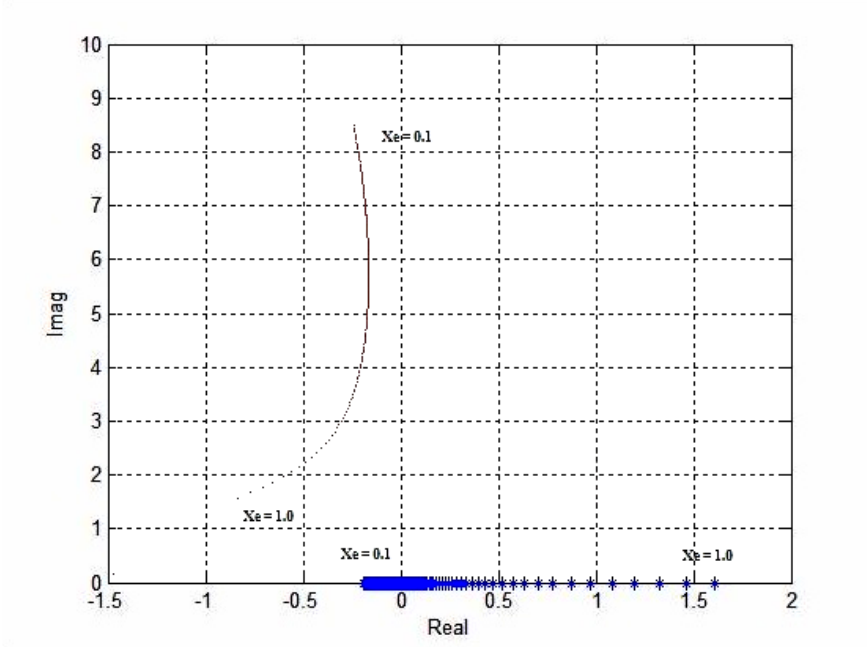

Fig.2.12 Eigenvalue loci for variation in x_e (0.1-1.0)

It is interesting to observe that

(i) The complex pair of eigenvalues corresponding to low frequency rotor oscillations is affected by AVR in different ways for cases (a) and (b). In the first case (Pg = 0.5), the damping is slightly increased with AVR while the frequency of oscillation is slightly decreased. This is equivalent to the statement that while AVR can contribute damping torque (with $K_5>0$) the synchronizing torque is slightly decreased.
For the case (b), the net damping becomes negative while the frequency of oscillation increases slightly. This is mainly due to fact that $K_5<0$, in this case.

(ii) There is a negative real eigenvalue in the case without AVR which moves towards the origin as P_g is increased. However the inclusion of a single time constant excitation system results in another complex pair in the left half plane, further away from the imaginary axis compared to the rotor mode. The loci of eigenvalues for the case without AVR are shown in Fig.2.11 as P_g is varied from 0.5 to 1.7. The variations with x_e (varied from 0.1 to 1.0) for Pg =1.0, are shown in fig.2.12. It is interesting to note that while the complex pair remains in the left half plane, the real eigenvalue crosses imaginary axis into RHP as either P_g or x_e is increased. This shows that instability in the case when AVR in absent, is mainly due to monotonic increase (or decrease) in the rotor angle when small perturbations are present.

2.5.2 Eigenvalue analysis for variation in AVR gain

Now, if we plot the curve for variation in AVR gain, then we need to vary K_E from 0 to 400.

(i) Here for case (a), the damping increases at first as K_E is increased from zero but starts decreasing as K_E is further increased. However the locus remains in the LHP.

(ii) For case (b), the damping starts decreasing as K_E is increased from zero and the eigenvalue crosses imaginary axis as K_E is increased beyond 17. Although the locus turns around as K_E is further increased, it remains in the RHP.

The difference in the loci for the two cases can be attributed to the fact that while $K_5<0$ for case (b) it is positive for case (a). Thus instability is expected in case (b) for sufficiently large values of K_E.

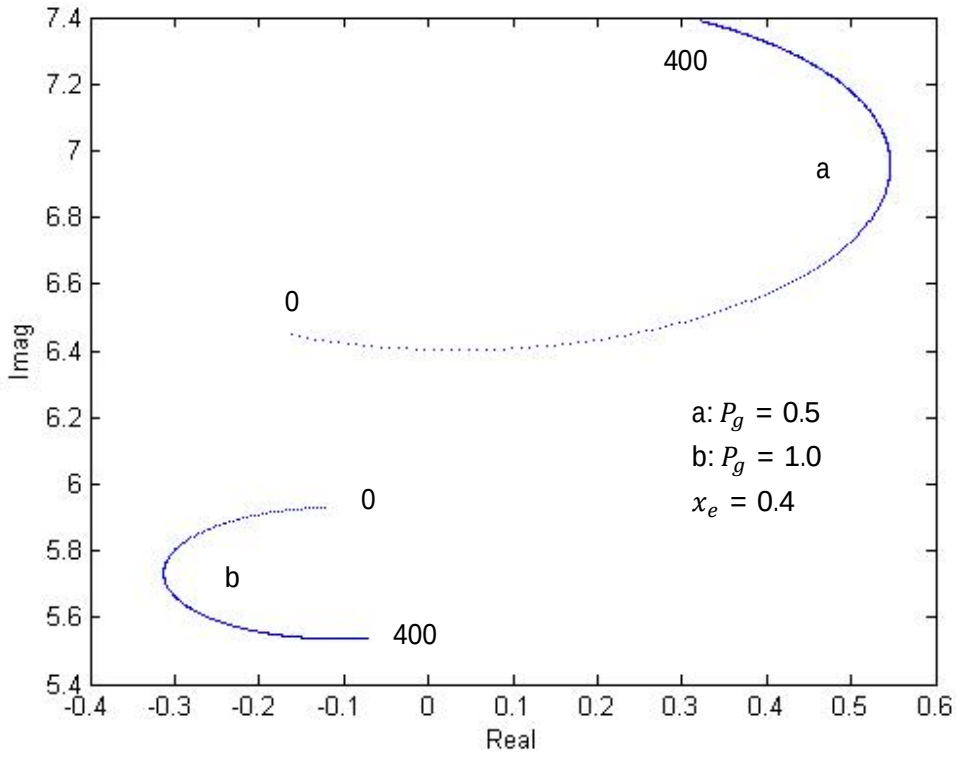

Fig.2.13 Eigenvalue loci for variation in AVR gain

Chapter 3

Modeling of a Grid connected DFIG

3.1 DFIG Equations in abc-Form

Here the convention is adopted for positive current, voltage and flux directions are shown in Fig.3.1.

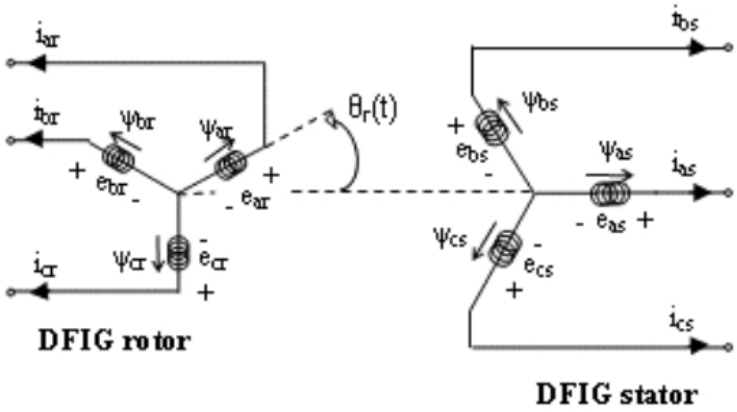

Fig.3.1. Definition of positive current, voltage and flux directions

As the machine is working in generator mode, positive currents are flowing out of it. The sign of the self-flux linkage produced by a current in a circuit is the same as that of the current. The polarity of the voltage induced by a changing flux is so that it results in a current that opposes the change (Lenz's law)
Applying the Kirchoff voltage law to Fig.3.1 gives:

$$V_{as} = -\frac{1}{\omega_B}\frac{d}{dt}\psi_{as} - R_s i_{as} \qquad (3.1)$$

where R_s, V_{as}, i_{as}, and ψ_{as} are in [pu] and are the stator phase-a winding resistance, voltage, current and flux linkage, respectively; ω_B [rad/sec] is the system base frequency which is equal to the synchronous frequency, i.e. $\omega_B = 2\pi f$, and t is the time in second and the flux ψ_{as} is:

$$\psi_{as} = (L_{self} + L_{leak})i_{as} + L_{mut}(i_{bs} + i_{cs}) + L_{sr}\left(\cos\theta_r i_{ar} + \cos\left(\theta_r + \frac{2\pi}{3}\right)i_{br} + \cos\left(\theta_r - \frac{2\pi}{3}\right)i_{cr}\right) \qquad (3.2)$$

Where $\theta_r = \theta_r(t)$ is the angle between the stator a-axis (stationary) and rotor a-axis (rotationary) as shown on Fig.3.1; L_{self} and L_{leak} are the self- and leakage inductance of a stator winding, respectively; L_{mut} is the mutual inductance between

two stator windings; and L_{sr} is the peak value of the mutual inductance between stator and rotor windings. For the other phases of the stator and rotor, similar equations can be written.

3.2 abc-dq transformation

In electrical engineering, direct-quadrature (dq) transformation is a mathematical transformation that rotates the reference system in an effort to simplify the analysis of three phase circuit. In the case of balanced three phase circuits, application of the dq transform reduces the three AC quantities to two DC quantities. Simplified calculations can then be carried out on these DC quantities.

3.2.1 Transformation matrix

For easier control, three-phase variables are transformed into dq variables. In matrix notation, we have:

$$v_{qd0} = T_\theta v_{abc} \tag{3.3}$$

where $v_{qd0} = [v_q \;\; v_d \;\; v_0]'$, $v_{abc} = [v_a \;\; v_b \;\; v_c]'$, and T_θ is the abc-to-dq transformation matrix. The power invariant transformation is chosen, and the d-axis is leading the q-axis. Fig.3.2 shows the dq-frame woth respect to the stator 3 axis frame. The corresponding transformation matrix is given in eqn. (3.4).

$$T_\theta = \sqrt{\frac{2}{3}} \begin{pmatrix} \sin\theta & \sin(\theta - \frac{2\pi}{3}) & \sin(\theta + \frac{2\pi}{3}) \\ \cos\theta & \cos(\theta - \frac{2\pi}{3}) & \cos(\theta - \frac{2\pi}{3}) \\ \frac{1}{\sqrt{2}} & \frac{1}{\sqrt{2}} & \frac{1}{\sqrt{2}} \end{pmatrix} \tag{3.4}$$

T_θ is orthogonal, thus the inverse transformation matrix is the transpose of T_θ.

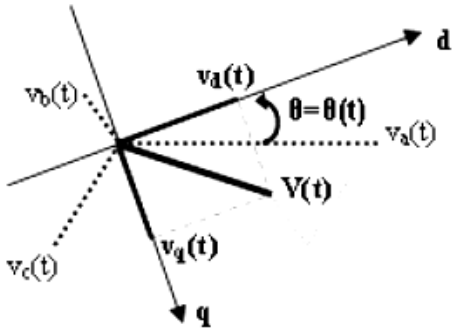

Fig.3.2 dq-frame with respect to stator abc-frame

3.2.2 DFIG equations in dq-form

Applying T_θ to eqn(3.1)-(3.2) and the other stator and rotor phase equations gives the DFIG dq-model in [pu]:

$$V_{qs} = -\frac{1}{\omega_B}\frac{d}{dt}\psi_{qs} - R_s i_{qs} + \omega\psi_{ds} \quad (3.5)$$

$$V_{ds} = -\frac{1}{\omega_B}\frac{d}{dt}\psi_{ds} - R_s i_{ds} - \omega\psi_{qs} \quad (3.6)$$

$$V_{qr} = -\frac{1}{\omega_B}\frac{d}{dt}\psi_{qr} - R_r i_{qr} + (\omega - \omega_r)\psi_{dr} \quad (3.7)$$

$$V_{dr} = -\frac{1}{\omega_B}\frac{d}{dt}\psi_{dr} - R_r i_{qr} - (\omega - \omega_r)\psi_{qr} \quad (3.8)$$

$$\psi_{qs} = L_{ss} i_{qs} + L_m i_{qr} \quad (3.9)$$

$$\psi_{ds} = L_{ss} i_{ds} + L_m i_{dr} \quad (3.10)$$

$$\psi_{qr} = L_{ss} i_{qr} + L_m i_{qs} \quad (3.11)$$

$$\psi_{qr} = L_{ss} i_{dr} + L_m i_{ds} \quad (3.12)$$

In eqn.3.5-3.8, ω_{is} the rotational speed of the dq-frame, i.e. $\omega = d\theta/dt$ where $\theta = \theta(t)$ is the angle between the d-axis and stator a-axis ; and ωr is the rotational speed of the rotor, i.e. $\omega_r = d\theta_r/dt$. For the synchronously rotating frame, ω is the synchronous speed, thus in [pu] $\omega = \omega_s = 1$ and $(\omega - \omega_r) = (\omega_s - \omega_r) = s\omega_s$ where s is the slip. In eqn.3.9-3.12, $L_{ss} = L_{self,s} + L_{leak,s} - L_{mut,s}$ and $L_m = L_{sr}$.

3.3 DFIG dq-Equations for Stability Studies

In a system to study stability, machines are represented as a voltage source behind transient impedance. Equations (3.5)-(3.12) can be rewritten so that the DFIG is represented as shown in fig.3.2. To this end, stator and rotor fluxes in (3.5)-(3.8) are eliminated with (3.9)-(3.12), and the following new variables are defined:

$$V_q' = (L_m/L_{rr})\,\omega_s\,\psi_{dr} \quad (3.13)$$

$$V_d' = -(L_m/L_{rr})\,\omega_s\,\psi_{qr} \quad (3.14)$$

$$X_s' = \omega_s\,(L_{ss}L_{rr} - L_m^2)/L_{rr} \quad (3.15)$$

$$T_0' = \omega_s L_{rr}/R_r \quad (3.16)$$

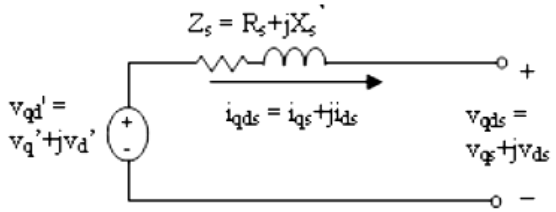

Fig.3.3 DFIG model for stability studies

After some derivations the DFIG-model in [pu] becomes:

$$\frac{X'_s}{\omega_S\,\omega_B}\frac{d}{dt}i_{qs} = -(R_s + \frac{Xs-X'_s}{T'_0})i_{qs} + X'_s i_{ds} + (1\text{-}s)v'_q - \frac{1}{T'_0}v'_d - v_{qs} + (L_m/L_{rr})v_{qr} \quad (3.17)$$

$$\frac{X'_s}{\omega_S\,\omega_B}\frac{d}{dt}i_{ds} = -(R_s + \frac{Xs-X'_s}{T'_0})i_{ds} - X'_s i_{qs} + (1\text{-}s)v'_d + \frac{1}{T'_0}v'_q - v_{ds} + (L_m/L_{rr})v_{dr} \quad (3.18)$$

$$\frac{1}{\omega_S\,\omega_B}\frac{d}{dt}v'_q = \frac{X_s-X'_s}{T'_0}i_{ds} - \frac{1}{T'_0}v'_q + sv'_d - \frac{Lm}{Lrr}v_{dr} \quad (3.19)$$

$$\frac{1}{\omega_S\,\omega_B}\frac{d}{dt}v'_d = -\frac{X_s-X'_s}{T'_0}i_{qs} - \frac{1}{T'_0}v'_d - sv'_q + \frac{L_m}{L_{rr}}v_{qr} \quad (3.20)$$

$$i_{qr} = -(1/\omega_s L_m)v'_d - (L_m/L_{rr})i_{qs} \quad (3.21)$$

$$i_{dr} = -(1/\omega_s L_m)v'_q - (L_m/L_{rr})i_{ds} \quad (3.22)$$

$$\psi_{qs} = -(1/\omega_s)v'_d + (X'_s/\omega_s)i_{qs} \quad (3.23)$$

$$\psi_{ds} = (1/\omega_s)v'_q + (X'_s/\omega_s)i_{ds} \quad (3.24)$$

3.4 Electromagnetic Torque

The instantaneous total active power produced by the DFIG is the sum of stator and rotor active powers:

$$P_{DFIG} = P_s + P_r \quad (3.25)$$

Where P_s and P_r are the real parts of $v_{qds}.i_{qds}^*$ and $v_{qdr}.i_{qdr}^*$ respectively. With $v_{qds} = v_{qs} + jv_{ds}$, $i_{qds} = i_{qs} + ji_{ds}$, $v_{qdr} = v_{qr} + jv_{dr}$ and $i_{qdr} = i_{qr} + ji_{dr}$, we have:

$$P_s = v_{qs}i_{qs} + v_{ds}i_{ds} \quad (3.26)$$

$$P_r = v_{qr}i_{qr} + v_{dr}i_{dr} \quad (3.27)$$

Substituting eqn. (3.5)-(3.8) in eqn. (3.26)-(3.27), gives:

$$P_{DFIG} = -R_s\left(i_{qs}^2 + i_{ds}^2\right) - R_r\left(i_{qr}^2 + i_{dr}^2\right)$$
$$-i_{qs}\frac{1}{\omega_B}\frac{d\psi_{qs}}{dt} - i_{ds}\frac{1}{\omega_B}\frac{d\psi_{ds}}{dt} - i_{qr}\frac{1}{\omega_B}\frac{d\psi_{qr}}{dt} - i_{dr}\frac{1}{\omega_B}\frac{d\psi_{dr}}{dt}$$
$$+\omega_s\psi_{ds}i_{qs} - \omega_s\psi_{qs}i_{ds} + s\omega_s\psi_{dr}i_{qr} - s\omega_s\psi_{qr}i_{dr} \quad (3.28)$$

The first two terms correspond to the machine losses, the second four terms to the power associated with flux variation, and the last four terms to the air gap power, i.e. the power converted from mechanical to electrical form.

The electromagnetic torque T_e is obtained by dividing the air gap power by the mechanical speed of the DFIG rotor. Doing this and using (3.9)-(3.12), gives in [pu]:

$$T_e = L_m(i_{qs}i_{dr} - i_{ds}i_{qr}) \tag{3.29}$$

Adding and subtracting the term $(L_m L_{rr}/L_{rr})i_{qs}i_{ds}$ gives the expression of T_e [pu] to be used with the DFIG model (3.5)-(3.12):

$$T_e = \left(\frac{L_m}{L_{rr}}\right)(i_{qs}\psi_{dr} - i_{ds}\psi_{qr}) \tag{3.30}$$

Substituting (3.13)-(3.14) in (3.30) gives another equivalent expression of T_e to be used with the DFIG model (3.17)-(3.24):

$$T_e = \left(\frac{v'_d}{\omega_s}\right) i_{ds} + \left(\frac{v'_q}{\omega_s}\right) i_{qs} \tag{3.31}$$

3.5 Drive Train Model

If the turbine, gearbox, generator, shafts and other transmission components are modeled as two masses Ht and Hg(with Ht> Hg) at the extremities of an equivalent common shaft, it follows from mechanics theory, that:

$$2H_t \frac{d\omega_t}{dt} = T_m - T_{sh} \tag{3.32}$$

$$2H_g \frac{d\omega_r}{dt} = T_{sh} - T_e \tag{3.33}$$

$$\frac{d\theta_{tw}}{dt} = (\omega_t - \omega_r)\omega_B \tag{3.34}$$

Where H_t and H_g [s] are the turbine and generator inertia, ω_t and ω_r [pu] are the turbine and DFIG rotor speed, and T_{sh} [pu] is the shaft torque:

$$T_{sh} = K\theta_{tw} + D\frac{d\theta_{tw}}{dt} \tag{3.35}$$

$$T_m = \frac{P_t}{\omega_t} \tag{3.36}$$

Where θ_{tw} [rad] is the shaft twist angle, K [pu/rad] the shaft stiffness, P_t [pu] is the turbine input power (here assumed as constant) and D [pu.s/rad] the damping coefficient. And T_e [pu] is generator torque that is given in eqn. (3.31).

3.6 Converter

The ac–dc–ac converter comprises of two pulse width modulation inverters connected back-to-back via a dc link. The rotor-side converter operates as a controlled voltage source since it injects an ac voltage at slip frequency to the DFIG rotor. The grid-side converter operates as a controlled current source since. It maintains the dc-link voltage constant and injects an ac current at grid frequency to the network [3].

The ac voltage of the rotor-side converter depends on the control objectives. For grid-connected WECS applications, a sensible choice is to impose a constraint for maximum power capture (equivalent to air gap power, electromagnetic torque, or speed constraint) and another for the voltage control (reactive power constraint). These two objectives determine the DFIG rotor voltage.

$\overline{V_r} = \overline{V_r}^{ref}$ So that $T_e = T_e^{ref}(\omega_r), \quad V_s = V_s^{ref}.$ (3.37)

For the grid-side converter, the control has to be coordinated so that the dc-link voltage is constant and the desired sharing of reactive power with stator is achieved. The reactive power sharing between the stator- and grid-side converters can be chosen arbitrarily. For minimum converter rating, as assumed in this pa-per, no sharing is done, and the reactive power delivered to the grid comes only from the stator. Hence, the grid-side converter ac current is such that the active power injected to the mains matches that of the rotor-side converter at unity power factor.

$\overline{I_{C2}} = \overline{I_{C2}}^{ref}$ So that $P_{C2} = P_r, \quad Q_{C2} = 0$ (3.38)

3.7 External Grid

To complete the model of the grid-connected DFIG, two more equations are required, namely the equations of the active and reactive power exchange between the grid and the generator. The external system is the infinite bus. Hence, the network algebraic equations are simply

$$P_{togrid} = \frac{V_s V_b sin\gamma_e}{X_e} \quad (3.39)$$

$$Q_{togrid} = \frac{V_s^2 - V_s V_b cos\gamma_e}{X_e} \quad (3.40)$$

Where the active and reactive powers delivered by the generator are $P_{togrid} = P_s + P_{C2}$ and $Q_{togrid} = Q_s + Q_{C2}$ with $P_{C2} = P_r$ and $Q_{C2} = 0$; V_s is the DFIG stator voltage magnitude; V_b and γ_e are the magnitude and angle of the infinite bus voltage; and X_e is the reactance of the external line.

3.8 DAE of the grid-connected DFIG

Initialization of the power system model is the starting point for both time-domain and frequency-domain analyses. This is done in two steps. First, the load flow calculation is done in order to obtain the voltage magnitude, voltage angle, and injected active and reactive powers at each bus. Then, with the obtained load flow solution, the generator is initialized by solving its set of differential algebraic equations (DAE) with all time derivatives set equal to zero.

3.8.1 Linearized Dynamic Model

The mathematical model of a power system can be written as a set of DAE

$$\frac{dx}{dt} = f(x, z, u) \tag{3.41}$$

$$0 = g(x, z, u) \tag{3.42}$$

Where x, z, and u are the state, algebraic, and input variables; f and g are the vectors of differential and algebraic equations, respectively. In small-signal analysis studies, (3.39) and (3.40) are linearized by a Taylor series expansion around an operating point(x0, z0, u0). Neglecting the terms of order two and above, and eliminating the algebraic variable z, the system state matrix is obtained as

$$A_{sys} = \left[\frac{\partial f}{\partial x} - \frac{\partial f}{\partial z}\left(\frac{\partial g}{\partial z}\right)^{-1} \frac{\partial g}{\partial x} \right]_{x_0, z_0, u_0} \tag{3.43}$$

The system dynamics is studied by examining the eigen-values of A_{sys}.

Here, $x = \left[i_{qs}\ i_{ds}\ v'_q\ v'_d\ \omega_r\ \theta_{tw}\ \omega_t \right]'$, $z = [V_s\ \gamma_e]'$, $u = \left[v_{qr}\ v_{dr}\ P_t \right]'$, f is contained in (3.17)–(3.20) and (3.32)–(3.34), and g is contained in (3.39) and (3.40). And $\frac{\partial f}{\partial x}, \frac{\partial f}{\partial z}, \frac{\partial g}{\partial x}, \frac{\partial g}{\partial z}$ matrices are derived as below:

$$\frac{\partial g}{\partial x} = \begin{pmatrix} v_{qs} - \frac{v_{qr} L_m}{L_{rr}} & v_{ds} - \frac{v_{dr} L_m}{L_{rr}} & 0 & 0 & 0 & 0 & 0 \\ v_{ds} - \frac{v_{dr} L_m}{L_{rr}} & -v_{qs} + \frac{v_{qr} L_m}{L_{rr}} & 0 & 0 & 0 & 0 & 0 \end{pmatrix}$$

$$\frac{\partial g}{\partial z} = \begin{pmatrix} \frac{-V_b \sin\gamma}{X_e} + i_{ds}\sin\gamma + i_{qs}\cos\gamma & \frac{-V_s V_b \cos\gamma}{X_e} + i_{ds} V_s \cos\gamma - i_{qs} V_s \sin\gamma \\ -\frac{2V_s}{X_e} + \frac{V_b \cos\gamma}{X_e} & -\frac{V_b V_s}{X_e}\sin\gamma \end{pmatrix}$$

$$\frac{\partial f}{\partial x}=\begin{pmatrix} -\frac{R_1\omega_e}{\omega_s L_s^{'}} & \omega_e & \frac{\omega_r\omega_e}{\omega_s^2 L_s^{'}} & -\frac{\omega_e}{T_r\omega_s^2 L_s^{'}} & 0 & 0 & \frac{\omega_e v_q^{'}}{\omega_s^2 L_s^{'}} \\ -\omega_e & -\frac{R_1\omega_e}{\omega_s L_s^{'}} & \frac{\omega_e}{T_r\omega_s^2 L_s^{'}} & \frac{\omega_r\omega_e}{\omega_s^2 L_s^{'}} & 0 & 0 & \frac{\omega_e v_d^{'}}{\omega_s^2 L_s^{'}} \\ 0 & R_2\omega_e & -\frac{\omega_e}{T_r\omega_s} & \left(1-\frac{\omega_r}{\omega_s}\right)\omega_e & 0 & 0 & -\frac{v_d^{'}\omega_e}{\omega_s} \\ -R_2\omega_e & 0 & -\left(1-\frac{\omega_r}{\omega_s}\right)\omega_e & -\frac{\omega_e}{T_r\omega_s} & 0 & 0 & \frac{v_q^{'}\omega_e}{\omega_s} \\ 0 & 0 & 0 & 0 & \left(-\frac{P_t}{2H_t\omega_t^2}-\frac{c\omega_{eB}}{2H_t}\right) & -\frac{k}{2H_t} & \frac{c\omega_{eB}}{2H_t} \\ 0 & 0 & 0 & 0 & \omega_{eB} & 0 & -\omega_{eB} \\ \frac{v_q^{'}}{2H_g\omega_s} & -\left(\frac{v_d^{'}}{\omega_s}\right)\frac{1}{2H_g} & -\frac{i_{qs}}{2H_g\omega_s} & -\frac{i_{ds}}{2H_g\omega_s} & \frac{c\omega_{eB}}{2H_g} & \frac{k}{2H_g} & -\frac{c\omega_{eB}}{2H_g} \end{pmatrix}$$

And

$$\frac{\partial f}{\partial z}=\begin{pmatrix} -\frac{\omega_e\cos\gamma}{\omega_s L_s^{'}} & \frac{V_s\omega_e\sin\gamma}{\omega_s L_s^{'}} \\ \frac{\omega_e\sin\gamma}{\omega_s L_s^{'}} & -\frac{V_s\omega_e\cos\gamma}{\omega_s L_s^{'}} \\ 0 & 0 \\ 0 & 0 \\ 0 & 0 \\ 0 & 0 \\ 0 & 0 \end{pmatrix}$$

Chapter 4
Results

4.1 Base-Case Modes

The SMIB system shown in Fig. 4.1 is studied. In the base case, the terminal voltage is 1 p.u., the total active power is 1 p.u., and the speed is at its rated value, which is assumed to be the synchronous speed. It is also assumed that the DFIG is directly connected to the infinite bus, i.e., the reactive power output is zero, and the terminal voltage remains constant. The effect of finite grid strength is investigated later. The base-case eigenvalues and their labeling are shown in Table 4.1(A). The modal oscillation frequency, damping ratio, and participation factors are shown in Table 4.1(B).The labeling of the modes are determined by observing the participation factors, as explained later.

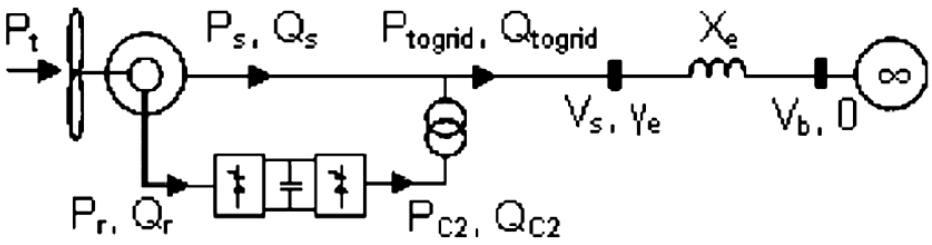

Fig.4.1 Power flows of the grid connected DFIG

	$\lambda = \sigma \pm j\omega$	Nature of the Mode
λ_1	-0.31 ±j3.38	Mechanical mode
λ_2	-8.01 ±j63.57	Electro-mechanical mode
λ_3	-16.16 ±j313.31	Stator mode
λ_4	-17.44	Non-oscillating mode

Table 4.1(A) Base case modes (Eigenvalue λ and nature of the mode)

	f_{osc}	ξ	p_{iqs}	p_{ids}	$p_{vq'}$	$p_{vd'}$	$p_{\omega r}$	$p_{\theta tw}$	$p_{\omega t}$
λ_1	0.54	0.092	.00	.00	.00	.01	.00	**.49**	**.50**
λ_2	10.12	0.125	.02	.01	.01	**.47**	**.46**	.01	.00
λ_3	49.86	0.052	**.48**	**.46**	.02	.03	.00	.00	.00
λ_4	0	1	.00	.01	**.98**	.01	.00	.00	.00

Table 4.1(B) Oscillation frequency, damping ration and participation factors

The base case has four stable modes, three of which are oscillating. The participation factors show the physical nature of the modes: λ1 is a mechanical mode associated with the turbine and shaft dynamics (turbine speed and torsion angle); λ2 is an electromechanical mode associated with the rotor electrical and mechanical dynamics (q-axis flux and generator speed); λ3 is an electrical mode associated with the stator dynamics; and λ4 is a non oscillating mode associated with the rotor electrical dynamics (d-axis flux). The participation factors also show that the modes are decoupled since a particular state variable participates significantly in only one of the modes. The mechanical mode is the dominant mode. It has a very low frequency (∼0.5 Hz) with a reasonable damping ratio (∼10%). The electromechanical mode has a higher frequency (∼10 Hz) and a slightly better damping ratio. The stator mode has the lowest damping ratio. However, its time constant is small (large real-part magnitude) and its frequency is much higher and out of the range of interest.

4.2 Effect of parameters

4.2.1 Drive Train Parameters

Varying the values of stiffness and inertia while keeping all other parameters at their base-case values does not cause significant eigenvalue displacement of the electrical modes (stator and non-oscillating modes).

	$\lambda = \sigma \pm j\omega$	f_{osc}	ξ	$p_{vd'}$	$p_{\omega r}$	$p_{\theta tw}$	$p_{\omega t}$
NT	-8.23±j26.4	4.20	0.298	**.47**	**.22**	.03	**.26**
T	-0.48±j128.6	20.47	0.004	.03	**.27**	**.47**	**.22**

Table 4.2 NT and T modes for k = 50pu/el.rad, H_g = 1s, H_t = 1s

4.2.2 Generator parameters

Varying the stator resistance R_s while keeping all other parameters constant causes noticeable displacements for all eigenvalues. Fig. 4.2 shows the eigenvalue loci for R_s/X_m=1/800 to 1/100. As the stator resistance increases, all the oscillatingmodes are better damped since they move further away from the imaginary axis.

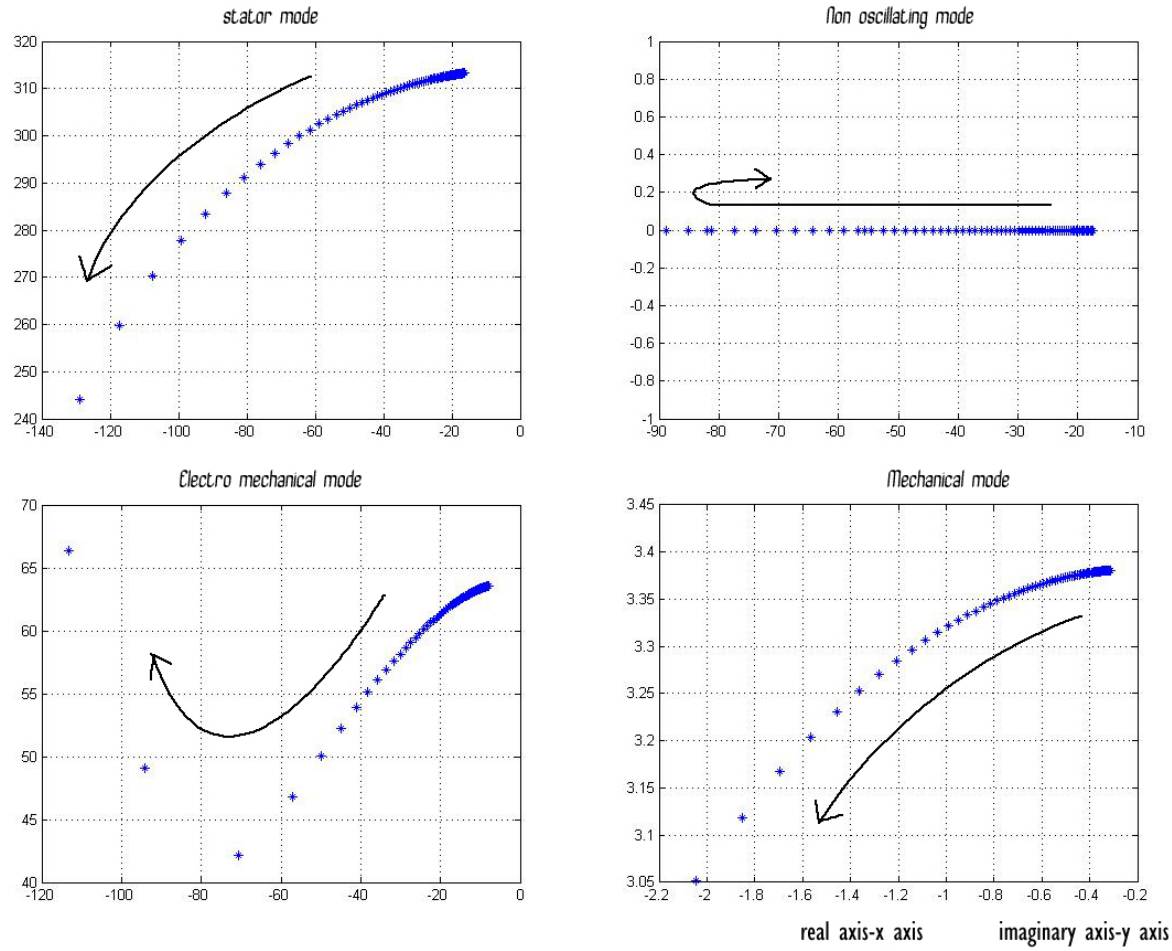

Fig 4.2 Eigenvalue loci for stator, electromechanical, non-oscillating and mechanical modes for increasing stator resistance (Rs/Xm = 1/800 to 1/100)

	$\lambda = \sigma \pm j\omega$	Nature of the mode
λ_1	-8.66±j4.69	Mechanical mode
λ_2	-50.61±j162.09	Electrical mode
λ_3	-469.59±j151.11	Electrical mode
λ_4	-2.60	Mechanical mode

Table 4.3 Eigenvalues and modes for very resistive machine (R_s/X_m = 1/50)

4.3 effect of the operating point

In this section, the effects of power production at non synchronous speeds, non unity power factors, and non unity terminal voltages are investigated.

4.3.1 Variation of Initial rotor speed and active power loading

The effect of initial rotor speed on the stator mode is not significant. For the non oscillating mode, the eigenvalue is the furthest away from the imaginary axis at synchronous speeds, while its absolute value decreases dramatically at non synchronous speeds. In fact, at large slip, the real eigenvalue is the dominant mode as shown in Table 4.4 for the operating point ω_r=0.7 p.u., P_{togrid} =0.35 p.u. In such a case, the system is over damped, and the oscillations are not an issue.

	$\lambda = \sigma \pm j\omega$	Nature of the mode
λ_1	-3.66±j8.55	Electro-mechanical mode
λ_2	-12.62±j112.43	Electro-mechanical mode
λ_3	-16.29±j312.94	Stator mode
λ_4	-1.21	Non-oscillating mode

Table 4.4 Modes for synchronous speed operation
(ω_r = 0.7 p.u. , P_{togrid} = 0.35 p.u.)

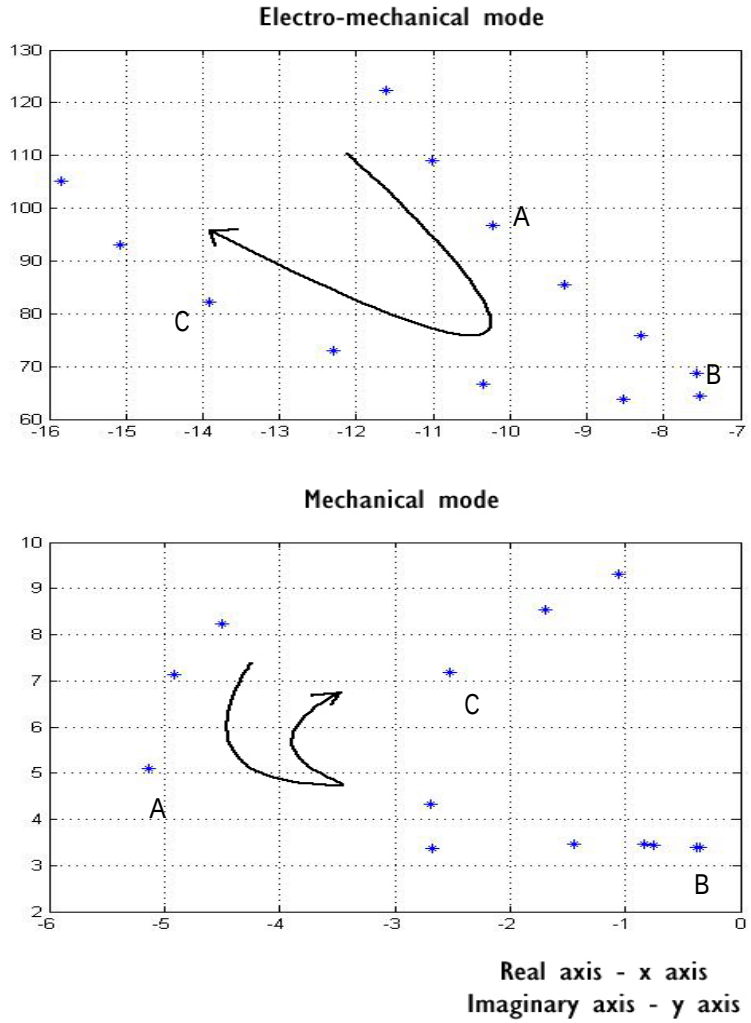

Fig 4.3 Eigenvalue loci of the electromechanical and mechanical modes for increasing rotor speed (ω_r = 0.67-1.3 pu).

Fig. 4.3 shows the eigenvalue displacement of the electro mechanical and mechanical modes. From a stability view point, small-slip speed (operating points around B) is the region of least stability. This also means that assuming the rated speed as synchronous is a more conservative approach. For the mechanical mode, the operating points A and C are the most stable for sub- and super synchronous speed operations, respectively. This means that in both the MPT and CPT regimes, there is an optimal speed for the stability of the critical mode.

4.3.2 Variation of Initial terminal voltage

The effect of voltage level is different in CPT and MPT conditions. Fig. 4.4 shows the eigenvalue displacement for in-creasing terminal voltages in the CPT regime (P_{togrid} =1p.u and $\omega_r=\omega_s$). The stator and the non oscillating modes are not significantly affected. For both electromechanical and mechanical modes, the oscillation frequency increases with the voltage as the magnitude of the imaginary part increases. In the CPT regime, the system is less stable for the overvoltage condition as the dominant mode (mechanical mode) moves closer to the imaginary axis.

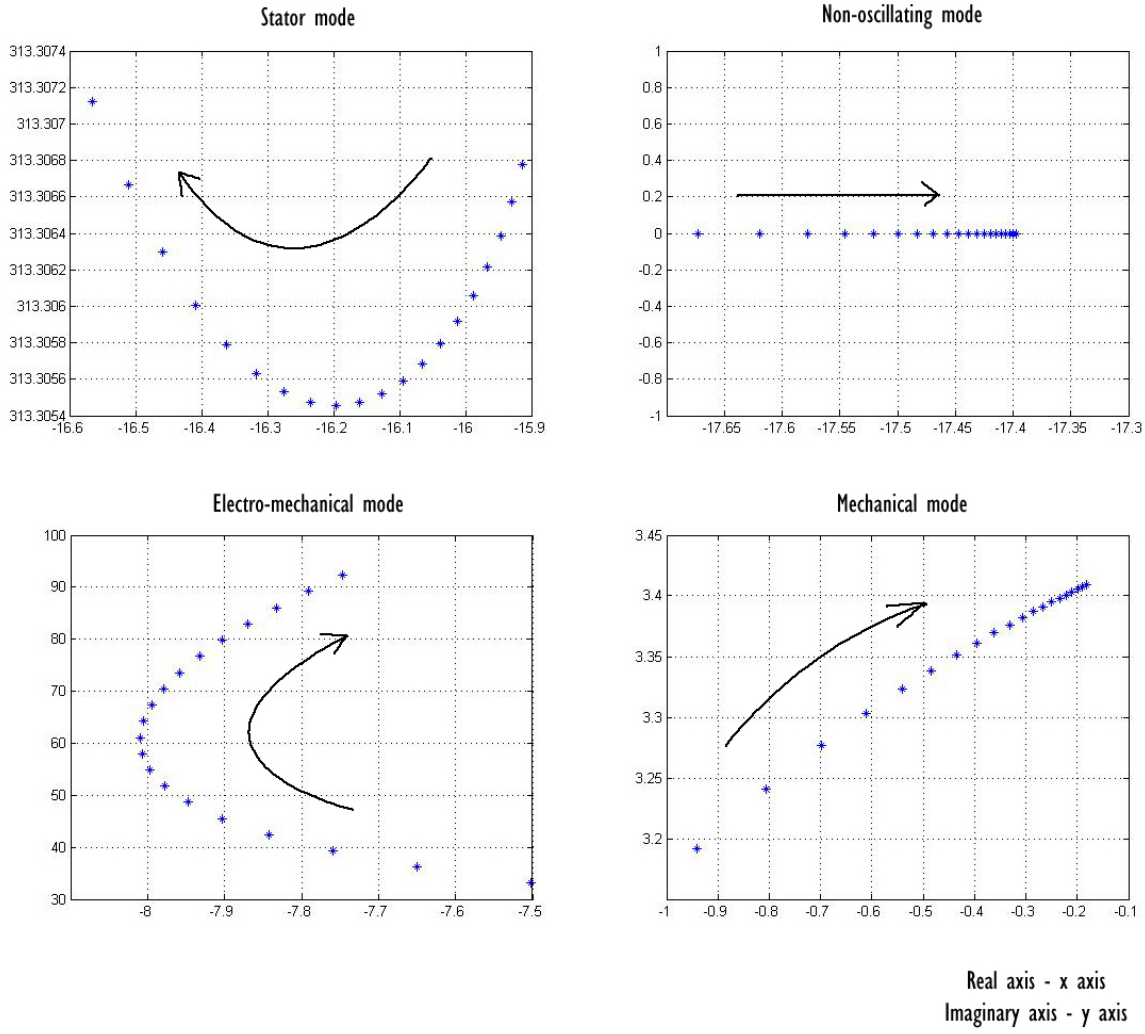

Fig 4.4 eigenvalue loci for increasing terminal voltage (V_s=0.5-1.5 pu) with P_{togrid} = 1 pu and Q_{togrid} = 0 pu.

And Fig. 4.5 shows the eigenvalue displacement for increasing terminal voltages in the MPT regime (P_{togrid} <1p.u. and $\omega_r<\omega_s$). The stator mode is not significantly affected. The electro mechanical and mechanical modes move toward the imaginary axis in an overvoltage condition indicating a less stable condition. For the depressed voltage condition ($V_s \leq 0.5$p.u.), the system is over damped.

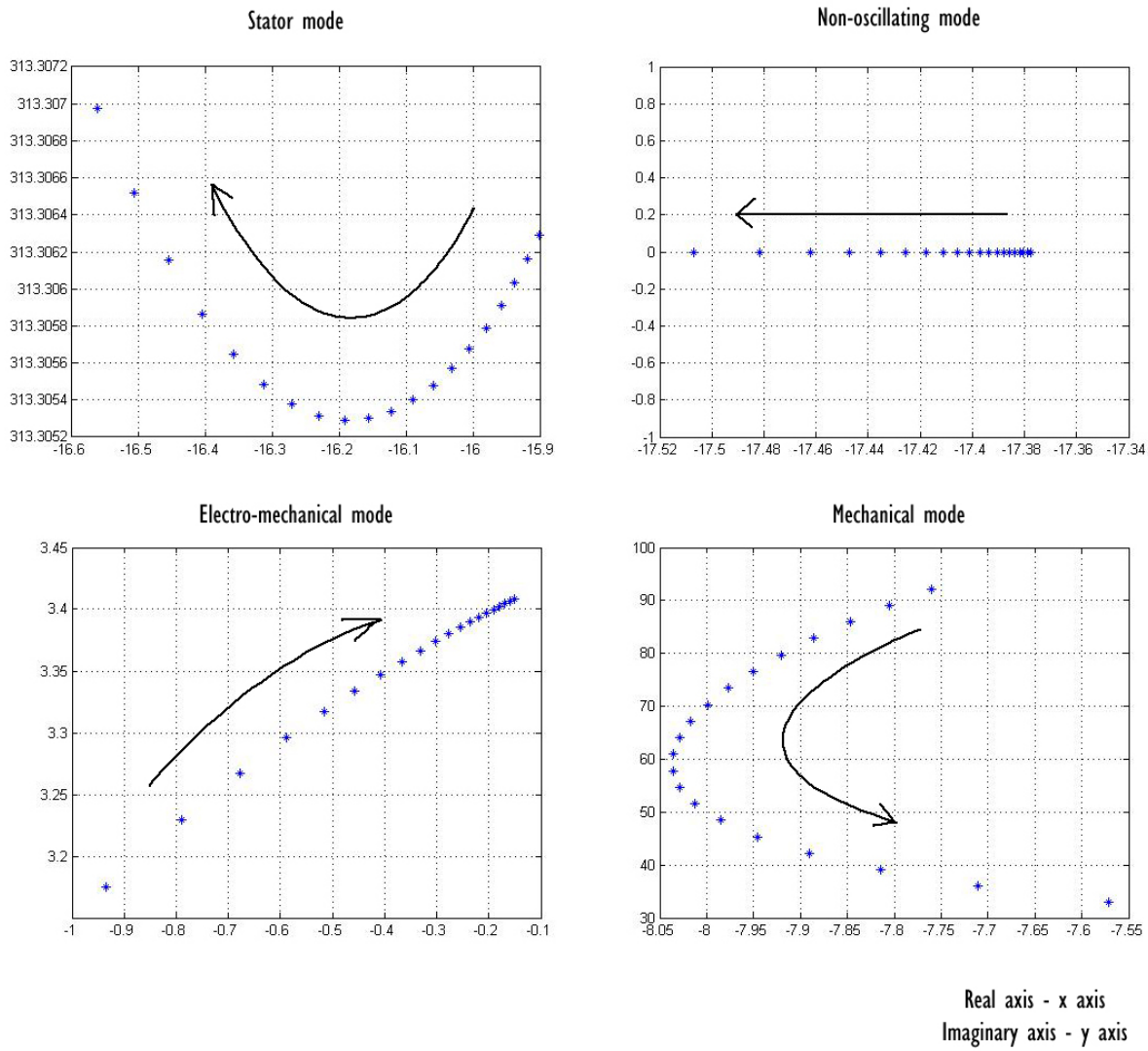

Fig. 4.5 Eigenvalue loci for increasing terminal voltage (V_s=0.5-1.5 pu) with P_{togrid} = 0.5 pu, Q_{togrid} = 0 pu.

4.3.3 Variation of External reactance

Fig. 4.6 shows the eigenvalue displacement for increasing external reactance X_e from 0 to 0.15 pu.

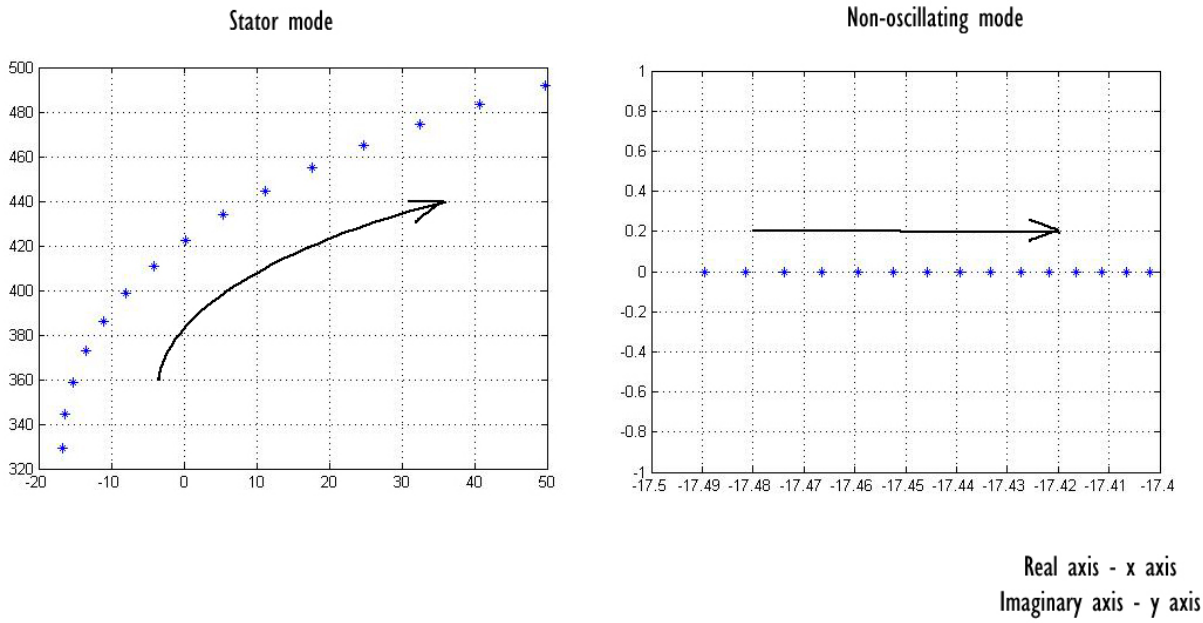

Fig. 4.6 Eigenvalue loci of the stator and non-oscillating modes for different values of external reactance (X_e = 0-0.15 pu)

4.4 Conclusion

This thesis presented the modal analysis of an SMIB system with DFIG. A seventh order model has been used with four state variables for the DFIG (stator and rotor dynamics) and three for the drive train (two-mass model). The results give the machine local modes, i.e., oscillations of the DFIG against the external system. The small-signal behavior is characterized by four modes, three of which are oscillating. The slowest mode (which is the dominant mode) is the drive-train non torsional mode. Oscillating at~0.5Hz, it is a mechanical mode associated with shaft and turbine dynamics. The second slowest mode is the drive-train torsional mode. Oscillating at~10Hz, it is an electromechanical mode associated with rotor dynamics (generator speed and rotor q-axis flux). The third oscillating mode is an electrical mode. Oscillating at~50Hz, it is associated with the stator dynamics. The non oscillating mode has a small time constant of~0.05s and is associated with the rotor d-axis flux dynamics. The effects of several parameters (drive-train inertias, stiffness, generator mutual inductance, and stator resistance), operating points (rotor speed, reactive power loading, and terminal-voltage level), and grid strength (external line reactance value) on the system modes have been studied.

The conditions for which stator dynamics can be neglected have also been provided. The results of this study offer a good starting point for the small-signal analysis of multi machine power systems with both conventional SG and wind-driven DFIG.

APPENDIX-A

A.1 Base case DFIG parameters

Turbine	Drive train	DFIG
P_t = 1 pu	k = 0.3 pu/el.rad	V_s = 1 pu
	c = 0	$R_s = X_m/800$
	H_t = 4s	$R_r = 1.1R_s$
	$H_g = 0.1H_t$	X_m = 4 pu
		$L_{ss} = 1.01L_m$
		$L_{rr} = 1.005L_{ss}$

References

[1] F. Mei, Bikash C. Pal, "Modeling and small-signal analysis of a grid connected doubly fed induction generator" in Power Engineering Society General Meeting, 2005, IEEE, 2101-2108 Vol.3.

[2] F. Mei, Bikash C. Pal, "Modal Analysis of Grid Connected doubly Fed Induction Generators" in IEEE transactions on energy conversion, Vol.22, No.3, September 2007.

[3] R. S. Pena, "vector control strategies for a doubly-fed induction generator driven by wind turbine" Ph.D. dissertation, Univ. Nottingham, Nottingham, U.K., 1996.

[4] J.G. Slootweg, H. Polinder, W.L. Kling, "Dynamic modelling of a wind turbine with doubly-fed induction generator," in Proc. 2001 IEEE Power Eng. Soc. Summer Meeting, vol. 1, pp 644-649.

[5] J.G. Slootweg, H. Polinder, W.L. Kling, "Initialization of Wind Turbine Models in Power System Dynamics Simulations" at PPT 2001 2001 IEEE Porto Power Tech Conference l0th -13th September, Porto, Portugal.

[6] Power system dynamics - Stability and control by K.R. Padiyar

[7] Power system stability and control by P. Kundur

[8] Elements of power system analysis by William D. Stevenson

[9] Power Systems Analysis by T.K. Nagsarkar, M.S. Sukhija

[10] Wind Power in Power Systems by Thomas Ackermann

[11] Renewable energy technologies – A practical guide for beginners by Chetan Singh Solanki.